High Power Laser Science and Engineering, (2024), Vol. 12, e16, 8 pages.
doi:10.1017/hpl.2023.100

HIGH POWER LASER SCIENCE AND ENGINEERING

RESEARCH ARTICLE

Generation of millijoule-level sub-5 fs violet laser pulses

Xinhua Xie[1], Yi Hung[2], Yunpei Deng[1], Adrian L. Cavalieri[1,3], Andrius Baltuška[2], and Steven L. Johnson[1,4]

[1]*SwissFEL, Paul Scherrer Institute, Villigen PSI, Switzerland*

[2]*Photonics Institute, Technische Universität Wien, Vienna, Austria*

[3]*Institute of Applied Physics, University of Bern, Bern, Switzerland*

[4]*Institute for Quantum Electronics, Physics Department, ETH Zurich, Zurich, Switzerland*

(Received 13 September 2023; revised 14 November 2023; accepted 14 December 2023)

Abstract

We demonstrate the generation, spectral broadening and post-compression of second harmonic pulses using a thin beta barium borate (BBO) crystal on a fused-silica substrate as the nonlinear interaction medium. By combining second harmonic generation in the BBO crystal with self-phase modulation in the fused-silica substrate, we efficiently generate millijoule-level broadband violet pulses from a single optical component. The second harmonic spectrum covers a range from long wave ultraviolet (down to 310 nm) to visible (up to 550 nm) with a bandwidth of 65 nm. Subsequently, we compress the second harmonic beam to a duration of 4.8 fs with a pulse energy of 0.64 mJ (5 fs with a pulse energy of 1.05 mJ) using chirped mirrors. The all-solid free-space apparatus is compact, robust and pulse energy scalable, making it highly advantageous for generating intense second harmonic pulses from near-infrared femtosecond lasers in the sub-5 fs regime.

Keywords: post-compression; second harmonic generation; self-phase modulation; supercontinuum generation

1. Introduction

The ultrafast dynamics of electrons and nuclei in atoms and molecules are crucial in describing their interaction with matter and light[1]. These dynamics occur over timescales ranging from picoseconds for nuclei to attoseconds for electrons[2–8]. In many applications, the use of ultrashort pulses is necessary to initiate and investigate specific dynamics through a pump–probe scheme. Typically, the temporal resolution of such pump–probe experiments depends on the pulse duration of both the pump and probe pulses. Therefore, achieving the required temporal resolution to resolve ultrafast dynamics in the time domain necessitates pump–probe pulses with comparable or shorter duration. Currently, mode-locked optical lasers and free-electron lasers (FELs) are routinely employed to generate ultrashort pulses, covering a broad spectral range from THz to hard X-rays[9–11]. Optical laser pulses can be delivered with durations as short as a few femtoseconds in the visible and near-infrared spectral range. These laser pulses can also be used to generate attosecond pulses in the extreme ultraviolet (UV)/soft X-ray spectral range through high-order harmonic generation[3].

Femtosecond pulses in the violet and UV spectral range can be generated through low-order harmonic generation of near-infrared femtosecond laser pulses from a Ti:sapphire or Yb-based laser amplifier. These violet and UV pulses find a wide range of applications in fields such as physics, chemistry, biology and materials science, enabling the investigation of ultrafast processes occurring on picosecond and femtosecond timescales. Time-resolved violet and UV spectroscopy with sub-hundred femtosecond pulses provides access to processes involving nuclear dynamics in chemical reactions and biological phenomena. To resolve ultrafast proton or electron dynamics, violet and UV pulses with durations below 10 fs are required[12]. However, the violet and UV pulse duration in low-order harmonic generation is limited by the bandwidths of the near-infrared fundamental pulses, which generally support pulse durations of only tens of femtoseconds.

Sub-10 fs pulses with sufficient pulse energy are also useful for nonlinear optics applications. For example, previous

Correspondence to: Xinhua Xie, SwissFEL, Paul Scherrer Institute, Forschungsstrasse 111, 5232 Villigen PSI, Switzerland. Email: xinhua.xie@psi.ch

experiments have demonstrated that high harmonic generation with millijoule 400 nm pulses significantly increases the conversion efficiency compared to 800 nm pulses[13]. Simulations have indicated that isolated attosecond pulses can be generated using a 6.5 fs 400 nm pulse with a double optical gating technique[14]. Therefore, a millijoule-level sub-10 fs violet and UV pulse can serve as the driving source for generating intense isolated attosecond pulses through high harmonic generation.

The sub-10 fs regime in the violet and UV spectral range can be reached with subsequent spectral broadening and post-compression in addition to the low-order harmonic generation process. Spectral broadening is usually achieved through the effect of self-phase modulation (SPM), which occurs when strong laser pulses interact with a nonlinear medium, such as gases or transparent solids[15,16]. SPM is a time-domain Kerr effect, where the third-order nonlinear susceptibility of a medium introduces an effective index of refraction n_{eff} that depends on the pulse intensity $I(t)$, given by $n = n_0 + n_2 I(t)$, where n_0 represents the linear index of refraction. For most materials, n_2 is greater than zero, resulting in a lower phase velocity at the center of an ultrashort pulse compared to its edges. Consequently, new frequencies are generated throughout the pulse as it propagates through the medium. This approach is widely employed for spectral broadening and post-compression of laser pulses across a spectral range spanning from UV to mid-infrared[17].

The most commonly used techniques for achieving sub-10 fs pulse durations in the violet and UV spectral range rely on SPM in gas-filled waveguides[18–26]. Nibbering *et al.*[20] obtained 15 μJ, 8 fs, 400 nm pulses with spectrum broadening in a gas-filled hollow-core capillary. Similarly, Liu *et al.*[23,24] achieved 45 μJ output energy with a pulse duration of 7.5 fs at around 400 nm. Cheng *et al.*[25] realized sub-10 fs, 500 μJ output at 400 nm using a gas-filled hollow-core fiber with an input pulse energy of 1 mJ. However, these pulse post-compression techniques based on gas-filled waveguides have some disadvantages. Firstly, fluctuations and long-term changes in gas pressure inside the waveguides can introduce significant timing fluctuations and drift in the laser arrival time, which can be problematic for applications requiring timing stability, such as pump–probe experiments at FEL facilities. In addition, gas-filled waveguide setups are generally implemented in vacuum systems, adding bulk and complexity to the experimental setup. A newly developed all-solid free-space technique based on multi-plate spectral broadening can overcome these disadvantages[27–37]. This technique utilizes thin fused-silica plates with thicknesses of a few hundred micrometers to broaden the spectrum of the input pulse through cascaded SPM while avoiding breakdown and spatial distortion in the medium due to self-focusing and conical diffraction[38,39]. Liu *et al.*[30] used eight thin glass plates in a single pass to broaden the spectrum of 400 nm pulses and compressed them to 8.6 fs with a pulse energy of 120 μJ. More recently, Hu *et al.*[40] generated 7.8 μJ, 5.2 fs, 400 nm pulses using a two-stage thin-plate setup. In addition to the techniques based on SPM, there are other methods available for generating broadband violet pulses through second harmonic generation (SHG). Szabó and Bor[41], Kanai *et al.*[42] and Zhou *et al.*[43] employed a frequency domain SHG technique, which allowed for broadband frequency doubling, and they obtained a 7.5 fs 400 nm pulse with a pulse energy of 320 μJ. Here in this work, we demonstrate the generation of a millijoule-level broadband violet pulse using a single optical component for the SHG in a thin beta barium borate (BBO) crystal and SPM of the second harmonic beam in the fused-silica substrate of the crystal, and further pulse post-compression down to sub-5 fs pulse duration using a chirped-mirror compressor.

2. Experiments

A schematic view of the experimental setup is presented in Figure 1. The fundamental pulses are delivered from a Ti:sapphire laser amplifier (Coherent Legend Elite Duo HE+) with the following specifications: a center wavelength of 800 nm, a pulse energy of 20 mJ, a repetition rate of 100 Hz and a pulse duration of 30 fs. The beam diameter at $1/e^2$ intensity is 18 mm. After a beam splitter, a portion of the laser beam with a pulse energy of 8.1 mJ is focused by a lens with a focal length of 750 mm. A thin type I BBO crystal with a thickness of 50 μm and a clear aperture of 10 mm on a 2 mm fused-silica substrate (BBO on the front side) is placed after the lens and before the focus for SHG. After the BBO crystal, a broadband wavelength separator (high reflection from 350 to 450 nm and high transmission from 700 to 900 nm) is used to isolate the second harmonic beam. To avoid damage to the optical components, the BBO crystal is kept at a minimum distance of 150 mm in front of the laser focus. After the wavelength separator, the second harmonic beam is re-collimated with a silver concave mirror with a focal length of 500 mm and bounced eight times between pairs of chirped mirrors (Ultrafast Innovations CM82, bandwidth, 350–450 nm; nominal group-delay dispersion (GDD) per bounce, –40 fs^2) to introduce negative group-velocity dispersion (GVD). Final compression is achieved upon transmission through a pair of uncoated fused-silica wedges, where the optical path length of the second harmonic beam through the glass wedges can be tuned to compensate residual GVD. Finally, the compressed second harmonic beam is sent to a self-diffraction frequency-resolved optical gating (SD-FROG) device for the pulse duration characterization[44]. The output spectrum is measured using a grating spectrometer. In the experiment, the grating compressor of the fundamental beam from the Ti:sapphire amplifier was tuned to deliver the shortest pulse at the BBO/fused-silica plate to achieve the broadest spectrum of the second harmonic.

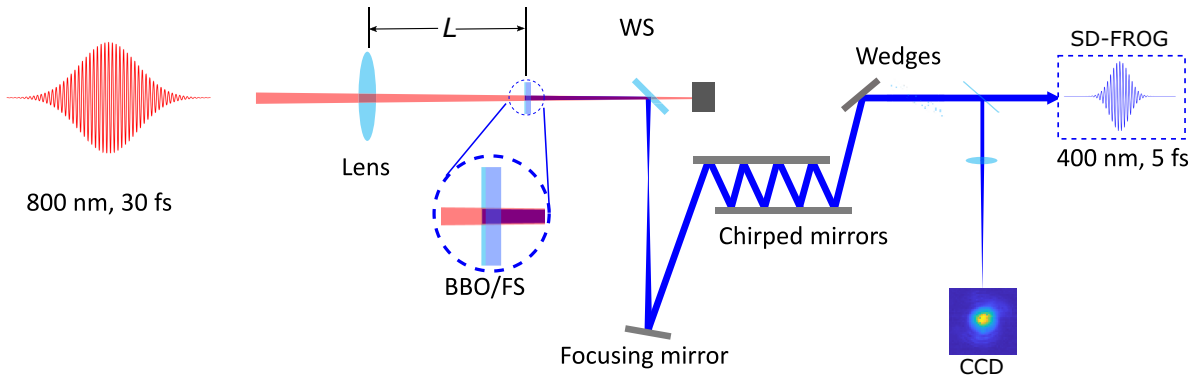

Figure 1. A schematic view of the experimental setup (WS, wavelength separator; FS, fused silica). The 800 nm beam is focused by a convex lens to the BBO crystal and its substrate. Afterward, the second harmonic beam is isolated and collimated before being sent to a chirped-mirror compressor. The beam profile was measured at the focus of an uncoated fused-silica lens with a focal length of 500 mm.

3. Results and discussion

3.1. Second harmonic generation and self-phase modulation

SHG and SPM are second- and third-order nonlinear processes, respectively. Therefore, the laser intensity plays a critical role in their efficiency. Efficient harmonic generation and effective spectral broadening due to SPM can only occur when the laser intensity is sufficient. In the experiment, an 800 nm laser beam was focused with a 750 mm focal length convex lens and the position of the lens was scanned with respect to the BBO/fused-silica plate to vary the laser intensity. The resultant SHG is characterized for different input intensities in Figure 2. The spectral dependence on input intensity (or distance L from the focusing lens) is shown in Figure 2(a). The integrated SHG signal strength and the SHG bandwidth at full width at half maximum (FWHM) are shown in Figure 2(b). When the BBO crystal is closer to the laser focus (increasing L) with higher intensity, a second harmonic beam with monotonically increasing signal intensity and bandwidth is observed. The signal intensity of the second harmonic beam can be increased by a factor of 4 until saturation, which is reached when L approaches 600 mm, with a corresponding pulse energy of 1.5 mJ measured after the wavelength separator. In the distance range between 350 and 600 mm, the bandwidth of the second harmonic signal increases quadratically.

The individual spectra of the second harmonic at three different positions are depicted in Figure 2(c). When the BBO crystal is far from the focus with $L = 100$ mm, the peak laser intensity (the maximum pulse intensity at the beam center) of the fundamental beam is approximately 2.7×10^{11} W/cm^2, and the spectral width of the second harmonic beam is about 19 nm, which is the same as that obtained with an unfocused fundamental beam. The onset of SPM occurs around $L = 350$ mm, corresponding to a peak laser intensity of 1.3×10^{12} W/cm^2 for the second harmonic beam in the fused silica. When the BBO crystal is moved to $L = 500$ mm, the spectrum becomes broader with an FWHM of 47 nm. The spectral bandwidth reaches 65 nm FWHM when $L = 600$ mm, which is significantly broader than that obtained with an unfocused beam, by a factor of more than 3. The fundamental beam is approximately 3.6 mm in diameter at $L = 600$ mm, resulting in a peak laser intensity of about 5×10^{12} W/cm^2 in the BBO. In the case of unsaturated SHG, the beam size of the second harmonic beam would be smaller than that of the fundamental beam with a ratio of $\sqrt{2}$. However, as indicated in Figure 2(b), the SHG is in saturation, and the diameter of the second harmonic beam is therefore larger than 2.6 mm. Taking the beam diameter into account and with a pulse energy of 1.5 mJ, the intensity of the second harmonic beam in the fused silica is estimated to be lower than 1.8×10^{12} W/cm^2 (assuming a pulse duration of 30 fs for the second harmonic beam after the BBO crystal). To avoid damage to the BBO crystal and its substrate, the BBO at the position was kept with $L = 600$ mm and the broadened second harmonic emission was used for subsequent pulse compression.

Intuitively, two possible scenarios can explain the spectral broadening of the second harmonic in the experiment. The first scenario involves a single step in which SHG and spectral broadening occur in the BBO crystal itself. The second scenario involves two steps: SHG in the BBO crystal and then spectral broadening of the SHG in the fused-silica substrate. To rule out the first scenario, the second harmonic spectrum was measured from a free-standing 100 μm BBO crystal without a substrate at the high-intensity position of $L = 600$ mm. The spectral width of the second harmonic is about 19 nm (FWHM), which matches the unbroadened spectral width obtained when using the 50 μm BBO/fused-silica plate at low intensity. This observation implies that there is no spectral broadening of the second harmonic signal in the BBO crystal. Therefore, it is found that spectral broadening occurs in the fused-silica substrate after the generation of the second harmonic beam from the BBO crystal.

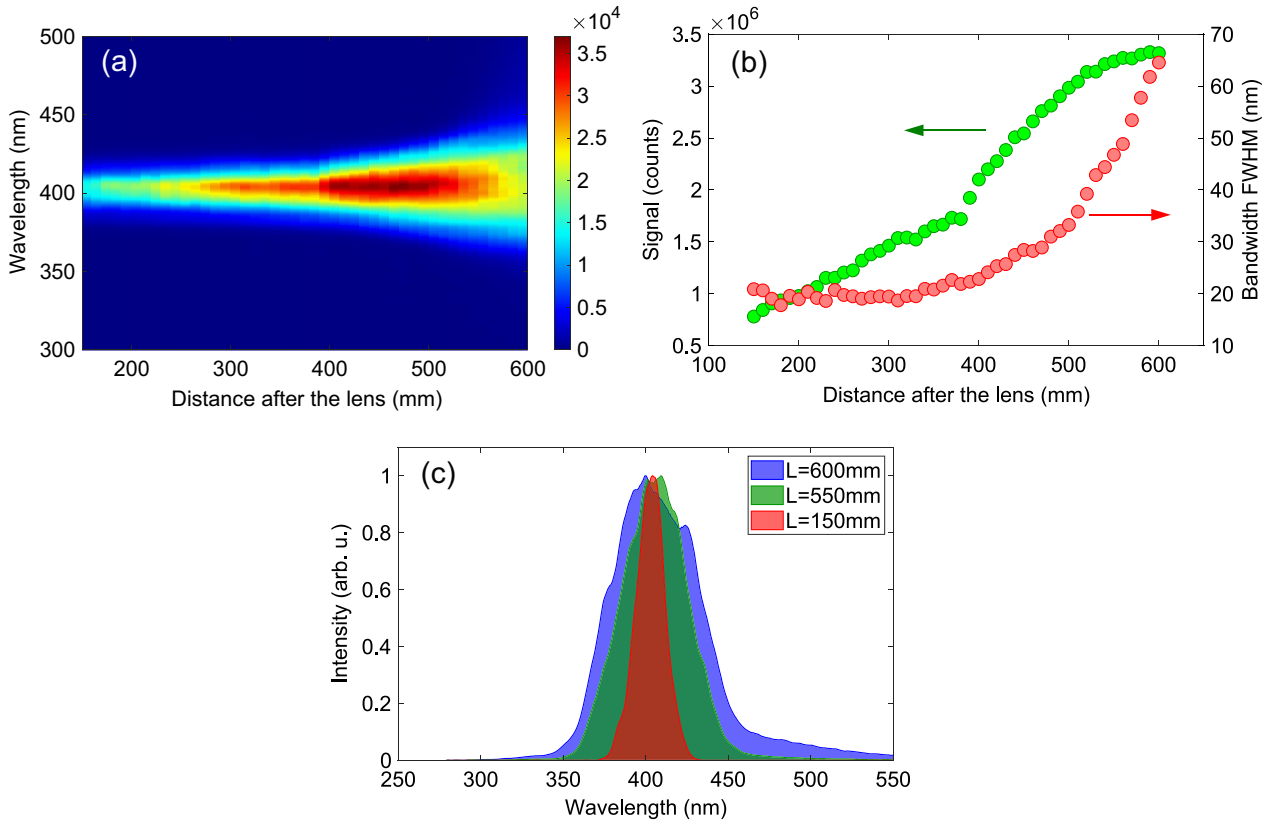

Figure 2. (a) Measured spectrum distribution as a function of the BBO position with respect to the focusing lens. (b) The bandwidth (FWHM) and the signal intensity of the second harmonic beam as a function of the BBO position with respect to the focusing lens. (c) Measured spectra of the second harmonic beam for three different BBO positions.

This conclusion is further supported by the fact that similar spectral broadening is also achieved when using the 100 μm free-standing BBO crystal at $L = 400$ mm and a 2 mm fused-silica plate placed afterward at $L = 600$ mm. Furthermore, the quadratic increase of the bandwidth as a function of the distance L after the lens, shown in Figure 2(b), can be explained by SPM. The spectrum broadening of SPM is proportional to the Kerr effect induced phase shift, which is expressed by the so-called B-integral: $B = 2\pi n_2 Il/\lambda_0$, where λ_0 is the central wavelength, I represents the laser peak intensity and l is the thickness of the nonlinear medium[17]. The SHG signal exhibits a linear increase as a function of the distance L before saturation, as shown in Figure 2(b). On the other hand, the lens has a focusing effect that reduces the beam size and increases the laser peak intensity linearly with L. As a result, the peak intensity of the SHG beam inside the substrate increases quadratically as a function of the distance L, leading to the quadratic increase of the bandwidth induced by SPM.

Besides SPM, cross-phase modulation (XPM) can also contribute to spectral broadening, where the phase of the second harmonic beam is modulated by the Kerr effect induced by the 800 nm beam[45]. To evaluate the potential contribution from XPM, the broadened spectrum of the second harmonic beam was measured using the 100 μm free-standing BBO crystal with a wavelength separation after the BBO and a 2 mm fused-silica plate at $L = 600$ mm. In this case, only the second harmonic beam is present in the fused silica. The measured spectrum is about 62 nm, which is 3 nm narrower than the spectrum without the wavelength separation. This difference can be attributed to a minor effect of XPM. The fact that XPM plays only a minor role can be explained by the group-velocity mismatch between the fundamental and second harmonic beams (approximately 10 fs delay from the 50 μm BBO and 55 fs for each millimeter of fused silica). Therefore, the spectral broadening of the second harmonic beam in the experiment predominantly occurs due to SPM in the 2 mm fused-silica substrate.

3.2. *Pulse compression using chirped mirrors*

For the pulse compression, the second harmonic beam generated with the 50 μm BBO and 2 mm fused-silica substrate placed at a distance $L = 600$ mm from the 750 mm focusing lens was first collimated with a concave mirror. In this case, the SHG bandwidth is approximately 65 nm FWHM. The collimated second harmonic beam is sent through the chirped-mirror compressor, consisting of eight bounces on chirped mirrors with approximately –40 fs^2 GDD per bounce, which also further removes the

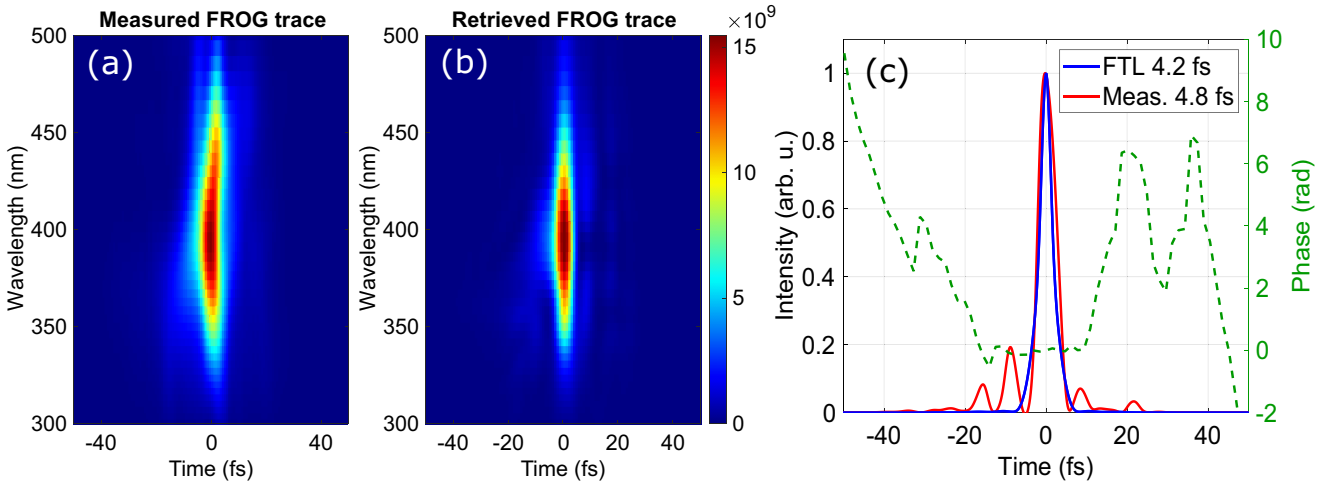

Figure 3. (a), (b) The measured and reconstructed SD-FROG traces. The reconstructed temporal intensity and phase of the pulse are shown in (c) together with the temporal profile of the Fourier-transform limited pulse.

residual fundamental beam. Finally, the beam is passed through the dispersion compensation wedge pair and then directed into an SD-FROG for pulse characterization. Using an iterative phase retrieval algorithm, the temporal shape of the measured pulse is reconstructed from the measured FROG trace[46]. The measured and reconstructed SD-FROG traces for the second harmonic pulse after compression are shown in Figures 3(a) and 3(b). The reconstructed pulse intensity envelope and phase are plotted in Figure 3(c). The reconstructed pulse exhibits an FWHM pulse duration of 4.8 fs, corresponding to less than four optical cycles, with the intensity of the pedestal below 20% of the main pulse. This duration is very close to the calculated Fourier-transform limited pulse duration of 4.2 fs, based on the measured spectrum. The pulse energy of the compressed pulse measures 640 μJ (1.14 mJ before compression). The pulse compression efficiency is approximately 56%. The significant loss in pulse energy is primarily due to two-photon absorption in the dielectric coating of the chirped mirrors when the laser fluence is high. In this case, the reflectivity of the chirped mirrors is 93%, although the design target is expected to be better than 99%. To increase the compression efficiency, either a different mirror design or a significant reduction in fluence is necessary. The total conversion efficiency from 800 nm to the compressed SHG is approximately 8%, which could be increased to about 14% by mitigating the two-photon absorption on the chirped mirrors.

3.3. Pulse energy scaling

The method demonstrated in this work is based on SHG in a BBO crystal and SPM in its fused-silica substrate. Pulse energy scaling can be achieved directly by adjusting the beam size on the BBO while maintaining the laser fluence. In the experiment, the input pulse energy was varied and the position of the BBO crystal was adjusted to achieve a spectral width of approximately 65 nm. The pulse duration and energy of the compressed pulses were measured. The compressed pulses exhibit durations of approximately 5 fs, similar to those obtained with input pulses of 8.1 mJ (Figure 3). The pulse energy of the compressed beam is plotted as a function of the fundamental pulse energy in Figure 4(a), clearly indicating a power scaling of the pulse energy of the compressed beam with respect to the pulse energy of the fundamental pulse. With an input pulse energy of 16 mJ, a compressed pulse with a pulse duration of 5 fs and a pulse energy of 1.05 mJ was achieved. Figure 4(b) summarizes the pulse duration and energy of the intense sub-10 fs 400 nm pulses demonstrated in this work and previous experiments with pulse energy higher than 100 μJ[25,30,42,43,47]. Our approach allows us to push the pulse duration of the 400 nm pulses into the sub-5 fs regime with a pulse energy at the millijoule level.

3.4. Beam stability

The stability of the laser fluence at the interaction point is a key parameter to achieve reliable time-resolved experiments, which is determined by the pulse energy and beam-pointing stability. Therefore, it is essential to maintain stable pulse energy and beam pointing during experiments. To measure the stability, single-shot measurements of the pulse energy and beam pointing of the compressed second harmonic beam were performed at 5-s intervals over 8 hours. Regarding energy stability, the laser amplifier exhibited a root mean square (RMS) stability of approximately 0.15% over 24 hours for the fundamental beam. Figure 5(a) presents the measured pulse energy of the second harmonic beam over 8 hours, with an RMS stability of 1.0%, which is sufficient for most time-resolved applications. The beam-pointing stability was evaluated by measuring the beam profile of the collimated beam with a charge-coupled device (CCD)

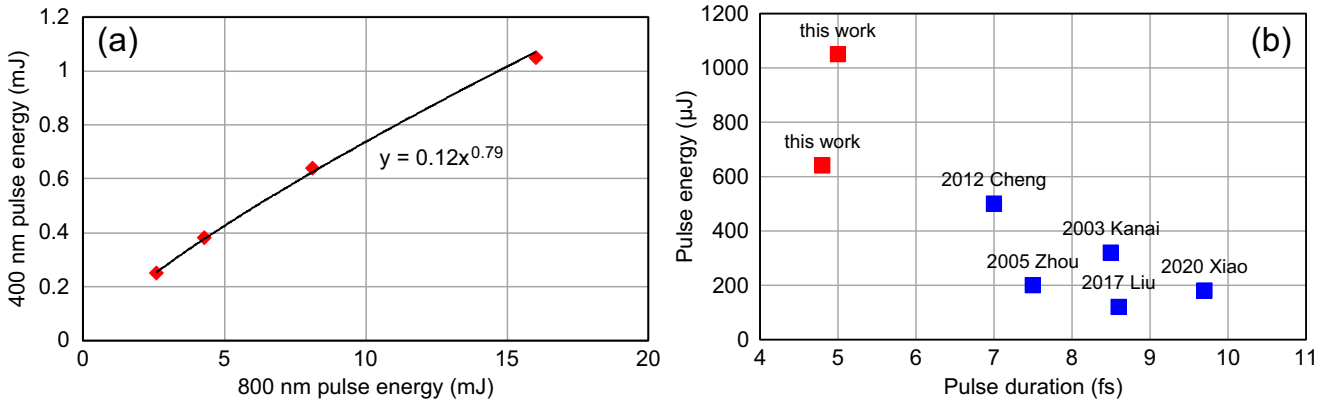

Figure 4. (a) The pulse energy of the compressed SHG pulse as a function of the fundamental pulse energy with a power function fitting. (b) A summary of pulse durations and energies for experimentally demonstrated intense sub-10 fs 400 nm pulses.

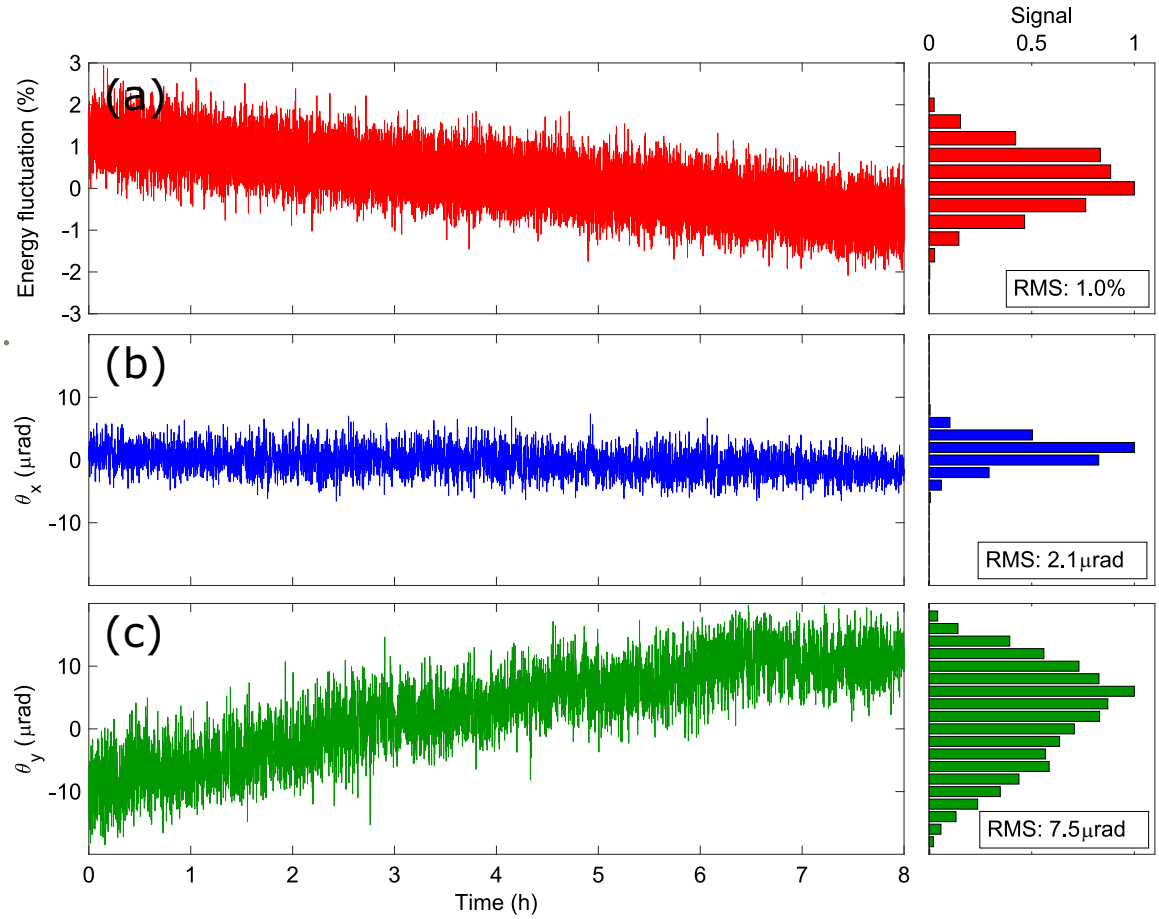

Figure 5. Single-shot measurements of pulse energy stability (a), and beam pointing along the horizontal (θ_x) and vertical (θ_y) directions (b), (c) over 8 hours for the compressed second harmonic beam. The histograms of the normalized stability distributions are plotted on the corresponding right-hand side panels.

camera at the focus through an uncoated fused-silica lens with a focal length of 500 mm, as shown in Figure 1. The 2D spatial distribution exhibits a Gaussian-like shape. The beam positions along the horizontal and vertical directions are determined by fitting the measured beam profile to a 2D Gaussian function. The angular pointing deviations are calculated by dividing the changes in the peak position by the focal length of the lens. The measured angular pointing stabilities of the compressed second harmonic pulses were 2.1 and 7.5 μrad (rms) along the horizontal and vertical directions, respectively, as shown in Figures 5(b) and 5(c). We observed that the beam pointing along the vertical direction has a drift over 8 hours, which could be due to the beam-pointing drift of the input beam. Such drift also

led to pulse energy dropping over 8 hours by about 1.5%. The beam-pointing drift can be compensated with a beam stabilization system before the SHG apparatus to improve the beam pointing and energy stability of the compressed second harmonic pulses.

4. Conclusion

In conclusion, we demonstrated the generation of millijoule-level sub-5 fs violet pulses from an all-solid free-space setup using a thin BBO crystal with a fused-silica substrate as the interaction medium. By harnessing the combined effects of SHG in the BBO crystal and SPM in the fused-silica substrate, we generated a broadband second harmonic beam with a bandwidth of 65 nm from a single optical component. Through the implementation of a chirped-mirror compressor, we compressed the broadened second harmonic pulses to a duration of 4.8 fs with a pulse energy of 0.64 mJ. Our method opens up new possibilities for generating intense violet and long wave UV pulses in the sub-5 fs regime, which holds great potential for a wide range of applications in nonlinear physics. For instance, it enables the generation of intense isolated attosecond pulses through high harmonic generation[13,14]. Our all-solid setup offers several advantages, including its compact size, robustness and scalability in terms of pulse energy. These characteristics make it an ideal solution for various applications that require intense, ultrashort violet or long wave UV pulses, particularly in the field of ultrafast time-resolved experiments. Importantly, the methodology we developed in this work has broader applications beyond the scope of this specific demonstration. The spectral broadening and pulse compression techniques we implemented can be potentially extended to the generation of broadband and ultrashort UV and visible pulses through the utilization of harmonic generation using thin nonlinear media. This paves the way for advances in a variety of fields that rely on intense ultrashort pulse sources, such as nonlinear optics, ultrafast spectroscopy and attosecond science.

References

1. A. Stolow, A. E. Bragg, and D. M. Neumark, Chem. Rev. **104**, 1719 (2004).
2. K. Yamanouchi, Science **295**, 1659 (2002).
3. F. Krausz and M. Ivanov, Rev. Mod. Phys. **81**, 163 (2009).
4. B. H. Bransden and C. J. Joachain, *Physics of Atoms and Molecules* (Pearson Education India, 2003).
5. X. Xie, K. Doblhoff-Dier, H. Xu, S. Roither, M. S. Schöffler, D. Kartashov, S. Erattupuzha, T. Rathje, G. G. Paulus, K. Yamanouchi, A. Baltuška, S. Gräfe, and M. Kitzler, Phys. Rev. Lett. **112**, 163003 (2014).
6. S. Erattupuzha, S. Larimian, A. Baltuška, X. Xie, and M. Kitzler, J. Chem. Phys. **144**, 024306 (2016).
7. X. Xie, S. Roither, D. Kartashov, E. Persson, D. G. Arbó, L. Zhang, S. Gräfe, M. S. Schöffler, J. Burgdörfer, A. Baltuška, and M. Kitzler, Phys. Rev. Lett. **108**, 193004 (2012).
8. X. Xie, K. Doblhoff-Dier, S. Roither, M. S. Schöffler, D. Kartashov, H. Xu, T. Rathje, G. G. Paulus, A. Baltuška, S. Gräfe, and M. Kitzler, Phys. Rev. Lett. **109**, 243001 (2012).
9. M. E. Fermann, A. Galvanauskas, and G. Sucha, *Ultrafast Lasers: Technology and Applications* (CRC Press, 2002).
10. C. Pellegrini, A. Marinelli, and S. Reiche, Rev. Mod. Phys. **88**, 015006 (2016).
11. E. A. Seddon, J. A. Clarke, D. J. Dunning, C. Masciovecchio, C. J. Milne, F. Parmigiani, D. Rugg, J. C. H. Spence, N. R. Thompson, K. Ueda, S. M. Vinko, J. S. Wark, and W. Wurth, Rep. Prog. Phys. **80**, 115901 (2017).
12. V. Hanus, S. Kangaparambil, S. Larimian, M. Dorner-Kirchner, X. Xie, M. S. Schöffler, G. G. Paulus, A. Baltuška, A. Staudte, and M. Kitzler-Zeiler, Phys. Rev. Lett. **123** (2019).
13. E. L. Falcão-Filho, C. J. Lai, K. H. Hong, V. M. Gkortsas, S. W. Huang, L. J. Chen, and F. X. Kärtner, Appl. Phys. Lett. **97**, 061107 (2010).
14. S. D. Khan, Y. Cheng, M. Möller, K. Zhao, B. Zhao, M. Chini, G. G. Paulus, and Z. Chang, Appl. Phys. Lett. **99**, 161106 (2011).
15. A. Dubietis, G. Tamošauskas, R. Šuminas, V. Jukna, and A. Couairon, Lith. J. Phys. **57**, 3541 (2017).
16. R. W. Boyd, *Nonlinear Optics* (Academic Press, 2020).
17. T. Nagy, P. Simon, and L. Veisz, Adv. Phys. X **6**, 1845795 (2021).
18. M. Nisoli, S. De Silvestri, and O. Svelto, Appl. Phys. Lett. **68**, 2793 (1996).
19. M. Nisoli, S. De Silvestri, O. Svelto, R. Szipöcs, K. Ferencz, C. Spielmann, S. Sartania, and F. Krausz, Opt. Lett. **22**, 522 (1997).
20. E. T. J. Nibbering, G. Korn, G. Tempea, and F. Krausz, Opt. Lett. **24**, 34 (1999).
21. F. Emaury, C. J. Saraceno, B. Debord, D. Ghosh, A. Diebold, F. Gèrôme, T. Südmeyer, F. Benabid, and U. Keller, Opt. Lett. **39**, 6843 (2014).
22. J. C. Travers, T. F. Grigorova, C. Brahms, and F. Belli, Nat. Photonics **13**, 547 (2019).
23. J. Liu, K. Okamura, Y. Kida, T. Teramoto, and T. Kobayashi, Opt. Express **18**, 20645 (2010).
24. J. Liu, Y. Kida, T. Kobayashi, and T. Teramoto, Opt. Express **18**, 4664 (2010).
25. Y. Cheng, S. D. Khan, B. Zhao, K. Zhao, M. Chini, and Z. Chang, in *Conference on Lasers and Electro-Optics* (2012), paper JW4A.23.
26. H.-T. Chang, M. Zürch, P. M. Kraus, L. J. Borja, D. M. Neumark, and S. R. Leone, Opt. Lett. **41**, 5365 (2016).
27. C.-H. Lu, Y.-J. Tsou, H.-Y. Chen, B.-H. Chen, Y.-C. Cheng, S.-D. Yang, M.-C. Chen, C.-C. Hsu, and A. H. Kung, Optica **1**, 400 (2014).
28. S. Hädrich, M. Kienel, M. Müller, A. Klenke, J. Rothhardt, R. Klas, T. Gottschall, T. Eidam, A. Drozdy, P. Jójárt, Z. Várallyay, E. Cormier, K. Osvay, A. Tünnermann, and J. Limpert, Opt. Lett. **41**, 4332 (2016).
29. P. He, Y. Liu, K. Zhao, H. Teng, X. He, P. Huang, H. Huang, S. Zhong, Y. Jiang, S. Fang, X. Hou, and Z. Wei, Opt. Lett. **42**, 474 (2017).
30. Y.-Y. Liu, K. Zhao, P. He, H.-D. Huang, H. Teng, and Z.-Y. Wei, Chin. Phys. Lett. **34**, 074204 (2017).
31. C.-H. Lu, T. Witting, A. Husakou, M. J. J. Vrakking, A. H. Kung, and F. J. Furch, Opt. Express **26**, 8941 (2018).
32. C.-H. Lu, W.-H. Wu, S.-H. Kuo, J.-Y. Guo, M.-C. Chen, S.-D. Yang, and A. H. Kung, Opt. Express **27**, 15638 (2019).
33. P. A. Carpeggiani, G. Fan, Z. Tao, G. Coccia, S. Zhang, Z. Fu, M. C. Chen, S. C. Liu, A. H. Kung, E. Kaksis, A. Pugzlys, and A. Baltuška, in *Laser Congress 2019* (2019), paper JTh3A.50.
34. M. Seo, K. Tsendsuren, S. Mitra, M. Kling, and D. Kim, Opt. Lett. **45**, 367 (2020).

35. H. Cao, R. S. Nagymihaly, N. Khodakovskiy, R. Lopez-Martens, V. Pajer, J. Bohus, B. Bussiere, F. Falcoz, A. Borzsonyi, and M. Kalashnikov, in *Laser Congress 2020* (2020), paper AW2A.2.
36. X. Xie, Y. Deng, and S. L. Johnson, High Power Laser Sci. Eng. **9**, e66 (2021).
37. S. Zhang, Z. Fu, B. Zhu, G. Fan, Y. Chen, S. Wang, Y. Liu, A. Baltuska, C. Jin, C. Tian, and Z. Tao, Light Sci. Appl. **10**, 53 (2021).
38. A. Couairon and A. Mysyrowicz, Phys. Rep. **441**, 47 (2007).
39. Y.-C. Cheng, C.-H. Lu, Y.-Y. Lin, and A. H. Kung, Opt. Express **24**, 7224 (2016).
40. F. Hu, Q. Zhang, J. Cao, Z. Hong, W. Cao, and P. Lu, Opt. Lett. **47**, 389 (2022).
41. G. Szabó and Z. Bor, Appl. Phys. B **50**, 51 (1990).
42. T. Kanai, X. Zhou, T. Sekikawa, S. Watanabe, and T. Togashi, in *Conference on Lasers and Electro-Optics/Quantum Electronics and Laser Science Conference* (2003), paper CFA5.
43. X. Zhou, T. Kanai, D. Yoshitomi, T. Sekikawa, and S. Watanabe, Appl. Phys. B **81**, 13 (2005).
44. R. Trebino, *Frequency-Resolved Optical Gating: The Measurement of Ultrashort Laser Pulses* (Springer, 2002).
45. R. R. Alfano and P. P. Ho, IEEE J. Quantum Electron. **24**, 351 (1988).
46. D. J. Kane and R. Trebino, IEEE J. Quantum Electron. **29**, 571 (1993).
47. F. Xiao, X. Fan, L. Wang, D. Zhang, J. Wu, X. Wang, and Z. Zhao, Chin. Phys. Lett. **37**, 114202 (2020).